

Fundamentals of the orbit and response for TianQin

Xin-Chun Hu¹, Xiao-Hong Li¹, Yan Wang¹, Wen-Fan Feng¹, Ming-Yue Zhou¹, Yi-Ming Hu^{2,3}, Shou-Cun Hu^{4,5}, Jian-Wei Mei^{2,3} and Cheng-Gang Shao¹

¹ MOE Key Laboratory of Fundamental Physical Quantities Measurements, Hubei Key Laboratory of Gravitation and Quantum Physics, School of Physics, Huazhong University of Science and Technology, 1037 Luoyu Road, Wuhan 430074, China

² TianQin Research Center for Gravitational Physics, Sun Yat-Sen University, Zhuhai 519082, China

³ School of Physics and Astronomy, Sun Yat-Sen University, Zhuhai 519082, China

⁴ Key Laboratory of Planetary Sciences, Purple Mountain Observatory, Chinese Academy of Sciences, 8 Yuanhua Road, Nanjing 210008, China

⁵ University of Chinese Academy of Sciences, Beijing 100049, China

E-mail: ywang12@hust.edu.cn

March 5, 2018

Abstract.

TianQin is a space-based laser interferometric gravitational wave detector aimed at detecting gravitational waves at low frequencies (0.1 mHz – 1 Hz). It is formed by three identical drag-free spacecrafts in an equilateral triangular constellation orbiting around the Earth. The distance between each pair of spacecrafts is approximately 1.7×10^5 km. The spacecrafts are interconnected by infrared laser beams forming up to three Michelson-type interferometers. The detailed mission design and the study of science objectives for the TianQin project depend crucially on the orbit and the response of the detector. In this paper, we provide the analytic expressions for the coordinates of the orbit for each spacecraft in the heliocentric-ecliptic coordinate system to the leading orders. This enables a sufficiently accurate study of science objectives and data analysis, and serves as a first step to further orbit design and optimization. We calculate the response of a single Michelson detector to plane gravitational waves in arbitrary waveform which is valid in the full range of the sensitive frequencies. It is then used to generate the more realistic sensitivity curve of TianQin. We apply this model on a reference white-dwarf binary as a proof of principle.

Keywords: gravitational waves, space-borne detector, TianQin

1. Introduction

The first direct detection of gravitational waves (GWs) from a pair of stellar-mass black holes (GW150914) has been made by the two advanced detectors of the Laser Interferometer Gravitational-Wave Observatory (LIGO) [1]. This event opens the era of observational GW astronomy. Subsequently, several more GW events of stellar-mass

black hole binaries have been detected [2, 3, 4, 5]. The first detection of GWs from a pair of neutron stars associated with a gamma-ray burst (GW170817/GRB170817A) [6] has been made jointly by advanced LIGO and advanced Virgo [7] which marks a major breakthrough of the multi-messenger astronomy. In the future, KAGRA [8] and LIGO-India [9] will also join in the ground-based detector network. Developments for the upgraded ground-based detectors, namely Advanced LIGO plus [10, 11] and LIGO Voyager, as well as the next generation detectors, such as Einstein Telescope [12] and Cosmic Explorer [13], have already been initiated.

Lower frequency windows for the GW astronomy are awaiting to be opened. Pulsar timing array (PTA), as a promising experiment sensitive to the very low frequency ($10^{-9} - 10^{-6}$ Hz) GWs, has been continuously improving its sensitivity for stochastic background produced by the incoherent superposition of GWs from a large ensemble of supermassive black hole binaries [14, 15, 16] and continuous waves from resolvable individual sources [17, 18, 19]. Prospects for GW astronomy with next generation large-scale PTAs based on FAST [20] and SKA [21] have been investigated [22].

Due to seismic noise and gravity gradient noise, it is very difficult to detect GWs with frequency lower than ~ 10 Hz by the ground-based detectors. It is a natural choice to deploy the laser interferometers in space [23]. There have been long-term studies and plots for the space-borne detectors to explore the low frequency regime (0.1 mHz – 1 Hz), where there is a very rich source of GWs [24]. LISA/eLISA [25, 26] is the most well studied one, especially with the successful demonstration of gravity reference system and space laser interferometry by the LISA Pathfinder [27]. The other space laser interferometric detectors, such as TianQin [28], DECIGO [29], g-LISA/GEOGRAWI [30, 31], ASTROD-GW [32, 33], TAIJI (ALIA descoped) [34], BBO [35, 36], OMEGA [37] and LAGRANE [38], are currently under various stages of research and development. A thorough overview of space-borne GW detectors can be found in [39].

During the initial study phase of the TianQin project, not all issues/complexities pertinent to the detector are fully recognized or anticipated. Work is now in progress to build prototype and end-to-end model to bring most of the issues into surface in order to avoid possible mistakes in the full development. The end-to-end model will utilize realistic simulations based on the feasible technologies to study the impact of different subsystems of the detector on the final high-precision measurements [40]. In principle, the elements of an end-to-end model will include the orbit of the spacecrafts [41], interplanetary and relativistic effects [42] on the optical links, various noises in a comprehensive noise budget, and the implementation of time delay interferometry (TDI) to reduce the laser phase noise and optical bench noise [43]. This model will aid in the design and optimization of the TianQin detector, so that it can meet the science requirements as launched.

The current work, as our first step toward building the end-to-end model, is to provide the mathematical formalism to represent the coordinates of the fiducial orbit for the TianQin's spacecraft. In the preliminary proposal [28], the TianQin detector is composed of three drag-free spacecrafts in an equilateral triangular constellation orbiting

around the Earth (see Fig. 1). The guiding center of the constellation coincides with the geocenter. The geocentric distance of each spacecraft is 1.0×10^5 km, which makes the distance between each pair of spacecrafts be 1.7×10^5 km. The period of the nearly circular Keplerian orbit of the spacecraft around the Earth is approximately 3.65 day. The spacecrafts are interconnected by infrared laser beams and form up to three (not independent) Michelson-type interferometers. The normal of the detector plane formed by the constellation points toward the tentative reference source RX J0806.3+1527 (also known as HM Cancr or HM Cnc), which is a candidate ultracompact white-dwarf binary in the Galaxy [44].

The time-varying spacecraft coordinates will be subsequently used in the forward modeling of the detector's response to the incident GWs. The calculation will be realized by the science data simulator module (e.g., LISACode [45] for LISA) in the end-to-end model, which is essentially used to convert the tensor GW perturbation to the scalar strain measurable by the detector. Noise components can also be added here. This simulator is crucial for studying the science objectives that can be enabled by TianQin [46] and testing the science data analysis techniques and pipelines of various GW sources.

The response of a space-based laser interferometer to GWs is not a straightforward extension of its ground-based counterparts. For the latter, geodesic deviation is used to calculate the proper distance change between two test masses. This treatment is valid only when the detector arm length L is shorter than the reduced wavelength of the passing GWs (i.e., under long-wavelength or low-frequency approximation) [47]. The critical wavelength corresponds to the so-called *transfer frequency* $f_* = c/(2\pi L)$. The sensitive GW frequency band is far below f_* for the ground-based detectors, but not for the space-based detectors. For frequencies higher than f_* (≈ 0.28 Hz for TianQin), the GW effect starts to cancel itself which in turn deteriorates the detector response. To obtain the time-varying detector response that is applicable in the whole frequency band, in principle one needs to integrate along the null geodesics of the photon that connect free-fall test masses [48]. However, this approach is computationally expensive. Instead, we adopt the *rigid adiabatic* approximation of the full response which is proven to have the high fidelity that meets the requirements of our subsequent work while significantly reduces the computational cost [49].

The rest of the paper is organized as follows. In Section 2, we present the coordinates for the orbit of TianQin's spacecraft, which are then used in the calculation of the detector response to gravitational waves and detector's sensitivity curve in Section 3. An example signal from the reference white-dwarf binary is given in Section 4. We conclude the main part of the paper in Section 5. Some calculation details have been relegated to the Appendix in order to allow the main ideas of the paper to be as clear as possible.

moon, planets (mostly Jupiter), large asteroids, etc. We give the components of the n -th spacecraft's position vector $\mathbf{r}_n(t) = (x_n(t), y_n(t), z_n(t))$ as a function of time in the heliocentric-ecliptic coordinate system below. The detailed derivation is relegated to Appendix A.

$$\begin{aligned}
x_n(t) &= R_1 \left(\cos \phi_s \sin \theta_s \sin(\alpha_n - \beta') + \cos(\alpha_n - \beta') \sin \phi_s \right) + R_1 e_1 \left[\frac{1}{2} (\cos 2(\alpha_n - \beta') - 3) \sin \phi_s \right. \\
&\quad \left. + \cos(\alpha_n - \beta') \cos \phi_s \sin \theta_s \sin(\alpha_n - \beta') \right] + \frac{e_1^2}{4} R_1 \sin(\alpha_n - \beta') \left[(3 \cos 2(\alpha_n - \beta') - 1) \right. \\
&\quad \left. \times \cos \phi_s \sin \theta_s - 6 \cos(\alpha_n - \beta') \sin(\alpha_n - \beta') \sin \phi_s \right] + R \cos(\alpha - \beta) + \frac{Re}{2} (\cos 2(\alpha - \beta) - 3) \\
&\quad - \frac{3Re^2}{2} \cos(\alpha - \beta) \sin^2(\alpha - \beta), \\
y_n(t) &= R_1 \left(\sin \phi_s \sin \theta_s \sin(\alpha_n - \beta') - \cos(\alpha_n - \beta') \cos \phi_s \right) - R_1 e_1 \left[\frac{1}{2} (\cos 2(\alpha_n - \beta') - 3) \cos \phi_s \right. \\
&\quad \left. - \cos(\alpha_n - \beta') \sin \phi_s \sin \theta_s \sin(\alpha_n - \beta') \right] + \frac{e_1^2}{4} R_1 \sin(\alpha_n - \beta') \left[(3 \cos 2(\alpha_n - \beta') - 1) \right. \\
&\quad \left. \times \sin \phi_s \sin \theta_s + 6 \cos(\alpha_n - \beta') \sin(\alpha_n - \beta') \cos \phi_s \right] + R \sin(\alpha - \beta) + \frac{Re}{2} \sin 2(\alpha - \beta) \\
&\quad + \frac{Re^2}{4} (3 \cos 2(\alpha - \beta) - 1) \sin(\alpha - \beta), \\
z_n(t) &= -R_1 \sin(\alpha_n - \beta') \cos \theta_s - R_1 e_1 \cos(\alpha_n - \beta') \sin(\alpha_n - \beta') \cos \theta_s \\
&\quad - \frac{1}{4} e_1^2 R_1 (3 \cos 2(\alpha_n - \beta') - 1) \sin(\alpha_n - \beta') \cos \theta_s, \tag{2}
\end{aligned}$$

where $R_1 = 1.0 \times 10^5$ km and e_1 are the semi-major axis and the eccentricity of the spacecraft orbit around the Earth; $R = 1$ AU and $e = 0.0167$ are the semi-major axis and the eccentricity of the geocenter orbit around the Sun. The normal of the detector plane formed by the spacecraft constellation points along the direction of $(\theta_s = -4.7^\circ, \phi_s = 120.5^\circ)$ which is the sky position of the reference source RX J0806.3+1527 in the ecliptic coordinates. Here $\alpha(t) = 2\pi f_m t + \kappa_0$ is the mean ecliptic longitude of the geocenter in the heliocentric-ecliptic coordinate system, $f_m = 1/(\text{one sidereal year}) = 3.14 \times 10^{-8}$ Hz is the modulation frequency due to the orbital motion around the Sun, and κ_0 is the mean ecliptic longitude measured from the vernal equinox at $t = 0$. β is the longitude of the perihelion. To obtain Eq. 2, we have introduced the detector coordinate system (see details in Appendix A) in which α_n is defined as the orbit phase of the n -th spacecraft in the detector plane and β' is the angle measured from the \tilde{x} axis in Fig. A1 to the perigee of the spacecraft. As stated in Appendix A, we have kept only up to the quadratic terms of the eccentricities e and e_1 here. Including higher order terms is straightforward.

Using Eq. 2, one can find that the instantaneous distance between the spacecraft i

and j is

$$\begin{aligned}
 L_{12}(t) &= \sqrt{3}R_1 \left[1 + \frac{e_1}{4} (\cos(\kappa - \beta') - \sqrt{3} \sin(\kappa - \beta')) \right. \\
 &\quad \left. + \frac{e_1^2}{32} (3\sqrt{3} \sin 2(\kappa - \beta') - 14 + 3 \cos 2(\kappa - \beta')) \right] + O(e_1^3), \\
 L_{13}(t) &= \sqrt{3}R_1 \left[1 + \frac{e_1}{4} (\cos(\kappa - \beta') + \sqrt{3} \sin(\kappa - \beta')) \right. \\
 &\quad \left. - \frac{e_1^2}{32} (3\sqrt{3} \sin 2(\kappa - \beta') + 14 - 3 \cos 2(\kappa - \beta')) \right] + O(e_1^3), \\
 L_{23}(t) &= \sqrt{3}R_1 \left[1 - \frac{e_1}{2} \cos(\kappa - \beta') - \frac{e_1^2}{16} (7 + 3 \cos 2(\kappa - \beta')) \right] + O(e_1^3), \tag{3}
 \end{aligned}$$

where $\kappa(t) = 2\pi f_{sc}t + \lambda$, $f_{sc} \approx 1/(3.65 \text{ day})$ is the modulation frequency due to the rotation of the spacecrafts around the guiding center, λ is the angle between the first ($n = 1$) spacecraft and \tilde{x} axis (see Fig. A1) at $t = 0$. We can see from Eq. 3 that to the leading order of e_1 the distance between two spacecrafts is $\sqrt{3}R_1 \approx 1.7 \times 10^5 \text{ km}$ which is the fiducial arm length of TianQin [28]. Note that a smaller e_1 is preferred to reduce the arm length variation during the mission. For example, one need to set $e_1 < 0.05$ when deploying the spacecraft in order to suppress the range rate of each arm below 15 m s^{-1} that is required by space interferometry [28].

Besides neglecting the higher order terms of the eccentricities, Eq. 2 has not yet included the correction term $\epsilon_n(t)$.

3. Detector Response

3.1. Description of gravitational waves

The plane GWs in arbitrary waveform can be decomposed into a spectrum of monochromatic waves with two independent polarizations, which can be expressed in the source frame as

$$\mathbf{h}(t, \mathbf{r}) = \int_{-\infty}^{+\infty} df \exp\left(i2\pi f(t - \hat{\Omega} \cdot \mathbf{r}/c)\right) \sum_{A=+, \times} \tilde{h}_A(f) \epsilon^A(\hat{\Omega}). \tag{4}$$

Here i is the imaginary unit, $\hat{\Omega}$ is the unit vector pointing along the direction of GW propagation and c is the speed of light. $\tilde{h}_A(f)$ ($A \in \{+, \times\}$) are the Fourier transforms of two GW polarizations. $\epsilon^A(\hat{\Omega})$ are the basis tensors, which are connected with the basis tensors $\mathbf{e}^A(\hat{k})$ defined in observer's frame via the polarization angle ψ in the standard spin-2 rotation transformation [50]

$$\begin{aligned}
 \epsilon^+(\hat{\Omega}) &= \mathbf{e}^+(\hat{k}) \cos 2\psi - \mathbf{e}^\times(\hat{k}) \sin 2\psi, \\
 \epsilon^\times(\hat{\Omega}) &= \mathbf{e}^+(\hat{k}) \sin 2\psi + \mathbf{e}^\times(\hat{k}) \cos 2\psi.
 \end{aligned} \tag{5}$$

Here $\hat{\Omega} = -\hat{k}$. $\mathbf{e}^A(\hat{k})$ can be formed by the unit vectors (\hat{p}, \hat{q})

$$\begin{aligned}
 \mathbf{e}^+ &= \hat{p} \otimes \hat{p} - \hat{q} \otimes \hat{q}, \\
 \mathbf{e}^\times &= \hat{p} \otimes \hat{q} + \hat{q} \otimes \hat{p},
 \end{aligned} \tag{6}$$

where \otimes is the tensor product, \hat{p} and \hat{q} reside in observer's plane of sky paralleling to the tangent vectors of θ and ϕ in the heliocentric ecliptic coordinate system, respectively. $(\hat{p}, \hat{q}, \hat{k})$ are orthonormal basis vectors which can be expressed as

$$\begin{aligned}\hat{p} &= (\cos \theta \cos \phi, \cos \theta \sin \phi, -\sin \theta) , \\ \hat{q} &= (\sin \phi, -\cos \phi, 0) , \\ \hat{k} &= (\sin \theta \cos \phi, \sin \theta \sin \phi, \cos \theta) .\end{aligned}\tag{7}$$

3.2. Detector response

For space-borne GW interferometer, the detector response, i.e. strain, is defined as the time variation of the differential optical path length of the two arms divided by the optical path length of one arm. Here, we adopt the rigid adiabatic approximation[‡] [49] to get the closed form of the strain output for the Michelson interferometer centered on spacecraft i

$$h_i(t) = \int_{-\infty}^{+\infty} df \exp\left(i2\pi f(t - \hat{\Omega} \cdot \mathbf{r}_i/c)\right) \sum_{A=+, \times} \tilde{h}_A(f) F_i^A(t; \hat{k}, f). \tag{8}$$

Here $F_i^A(t; \hat{k}, f)$ are called the *antenna pattern functions* which are generally functions of source direction \hat{k} and GW frequency f . They are defined by [50]

$$F_i^A(t; \hat{k}, f) \equiv \mathbf{D}_i(t; \hat{k}, f) : \boldsymbol{\epsilon}^A(\hat{\Omega}), \tag{9}$$

where the colon represents the double contraction of two rank-2 tensors, i.e., $\mathbf{A} : \mathbf{B} = A_{ij}B^{ij}$. \mathbf{D}_i is the *detector tensor* of the interferometer centered on spacecraft i

$$\mathbf{D}_i(t; \hat{k}, f) = \frac{1}{2} \left[\hat{r}_{ij}(t) \otimes \hat{r}_{ij}(t) \mathcal{T}(\hat{r}_{ij}(t), \hat{k}, f) - \hat{r}_{ik}(t) \otimes \hat{r}_{ik}(t) \mathcal{T}(\hat{r}_{ik}(t), \hat{k}, f) \right], \tag{10}$$

where $i, j, k \in \{1, 2, 3\}$ and $i \neq j \neq k$. $\hat{r}_{ij}(t)$ is the unit vector points from spacecraft i to spacecraft j . \mathcal{T} is the *transfer function* which can be written as [51]

$$\begin{aligned}\mathcal{T}(\hat{r}_{ij}(t), \hat{k}, f) &= \frac{1}{2} \left[\text{sinc}\left(\frac{f}{2f_*}(1 + \hat{k} \cdot \hat{r}_{ij}(t))\right) \exp\left(-i\frac{f}{2f_*}(3 - \hat{k} \cdot \hat{r}_{ij}(t))\right) \right. \\ &\quad \left. + \text{sinc}\left(\frac{f}{2f_*}(1 - \hat{k} \cdot \hat{r}_{ij}(t))\right) \exp\left(-i\frac{f}{2f_*}(1 - \hat{k} \cdot \hat{r}_{ij}(t))\right) \right],\end{aligned}\tag{11}$$

where $f_* = c/(2\pi L_{ij})$ is the transfer frequency. As we shall see in Sec. 3.3, in the frequency region that $f > f_*$ the detector response starts to oscillate and decay that partly cancel the GW effect in accord with the characteristics of \mathcal{T} . \mathcal{T} approaches unity if $f < f_*$, such that the detector tensor becomes dependent only on the geometric configuration of the interferometer. Note that f_* is not a constant due to the variation of the arm length induced by the breathing and flexing of the constellation.

[‡] The term ‘‘adiabatic’’ indicates that we approximate the continuous motion of the spacecraft constellation as a series of quasi-stationary state during the photon traveling time between two spacecrafts (equivalently taking stroboscopic images of the constellation).

We define a surrogate variable $\xi_i^A(t) = \mathbf{D}_i^A(t; \hat{k}, f) : \mathbf{e}^A(\hat{k})$. For $i = 1$

$$\begin{aligned}\xi_1^+(t; \theta, \phi) &= \frac{\sqrt{3}}{32} [4 \cos 2(\kappa - \beta') ((3 + \cos 2\theta) \sin \theta_s \sin 2(\phi - \phi_s) + 2 \sin(\phi - \phi_s) \sin 2\theta \cos \theta_s) \\ &\quad - \sin 2(\kappa - \beta') (3 + \cos 2(\phi - \phi_s) (9 + \cos 2\theta (3 - \cos 2\theta_s)) + 6 \cos 2\theta_s \sin^2(\phi - \phi_s) \\ &\quad - 6 \cos 2\theta \cos^2 \theta_s + 4 \cos(\phi - \phi_s) \sin 2\theta \sin 2\theta_s)] , \\ \xi_1^\times(t; \theta, \phi) &= \frac{\sqrt{3}}{8} [-4 \cos 2(\kappa - \beta') (\cos 2(\phi - \phi_s) \cos \theta \sin \theta_s + \cos(\phi - \phi_s) \sin \theta \cos \theta_s) \\ &\quad + \sin 2(\kappa - \beta') (\cos \theta (3 - \cos 2\theta_s) \sin 2(\phi_s - \phi) + 2 \sin(\phi_s - \phi) \sin \theta \sin 2\theta_s)] .\end{aligned}\tag{12}$$

The explicit expressions for $\xi_2^{+, \times}$ and $\xi_3^{+, \times}$ can be similarly obtained. Note that for simplicity we have set $e_1 = 0$ in Eq. 12, considering that $\xi_i^{+, \times}$ in expansion of e_1 are straightforward to derive but too lengthy to be shown here. Combining Eq. 5, Eq. 9 and $\xi_i^{+, \times}$, we can get

$$\begin{aligned}F_i^+(t; \theta, \phi, \psi) &= \cos 2\psi \xi_i^+(t; \theta, \phi) - \sin 2\psi \xi_i^\times(t; \theta, \phi) , \\ F_i^\times(t; \theta, \phi, \psi) &= \sin 2\psi \xi_i^+(t; \theta, \phi) + \cos 2\psi \xi_i^\times(t; \theta, \phi) .\end{aligned}\tag{13}$$

3.3. Sensitivity curve

The noise budget for the key components of the TianQin detector has been given in [28]. The main ones are the position noise (optical path noise) rooted from the photon shot noise at the measurement of laser phase by phasemeter and the acceleration noise rooted from the initial sensor in the disturbance reduction system. The preliminary goal for the amplitude spectral density (ASD) of these two noise sources are $\sqrt{S_x} = 1 \text{ pm/Hz}^{1/2}$ for each position measurement and $\sqrt{S_a} = 10^{-15} \text{ m s}^{-2}/\text{Hz}^{1/2}$ for each interaction with inertial sensor, respectively. These two noises can be essentially regarded as white in the interested frequency range, except that the inherent $1/f$ noise will emerge from the inertia sensor for $f < 10^{-4} \text{ Hz}$.

The position noise from each phasemeter measurement is uncorrelated. Thus simply summing over the power spectral density (PSD) contribution from each phasemeter in the optical path gives the total PSD. The equivalent strain noise ASD $\sqrt{S_n^x}$ can be obtained through dividing the total position noise ASD by the optical path length of $2L$ on one arm, which gives

$$S_n^x = \left(\frac{\sqrt{4S_x}}{2L} \right)^2 = \frac{S_x}{L^2} .\tag{14}$$

The factor of four in the numerator is due to the fact that there are two phasemeter measurements on each arm (one at the transmitting spacecraft, one at the responding spacecraft) which add up to four measurements for the Michelson interferometer.

Similarly one can calculate the equivalent strain noise due to acceleration noise. Note that the acceleration noise acts coherently on the incoming and outgoing laser, which gives a combined $2\sqrt{S_a}$ for each inertial sensor on board of a spacecraft. There are four contributions for an interferometer. Dividing the total acceleration noise ASD

by $(2\pi f)^2$ gives the equivalent position noise ASD, further dividing it by $2L$ gives the equivalent strain noise ASD,

$$S_n^a = \left(\frac{\sqrt{16S_a}}{(2\pi f)^2 \cdot 2L} \right)^2 = \frac{4S_a}{(2\pi f)^4 L^2}. \quad (15)$$

Following [28] we have the ASD of the effective strain noise (in unit of $1/\sqrt{\text{Hz}}$)

$$h_n(f) = \frac{1}{\sqrt{R(f)}} \left[S_n^x + S_n^a \left(1 + \frac{10^{-4} \text{ Hz}}{f} \right) \right]^{\frac{1}{2}}, \quad (16)$$

here the multiplier associated with S_n^a is owing to the $1/f$ noise of the inertial sensor. The function $R(f)$ is defined as follows [52],

$$R(f) = \int \frac{d\hat{k}}{4\pi} \sum_A F^A(t; \hat{k}, f) F^A(t; \hat{k}, f)^*, \quad (17)$$

which is an all-sky average for the sum of squared amplitudes of the antenna pattern functions. Note that the polarization angle ψ has been self canceled in the integrand. Based on Eq. 14–17, the sensitivity curve, i.e., h_n of TianQin is calculated and presented in Fig. 2. The red dash line represents an analytic approximation of $R(f)$ [52] which is in a good agreement with the approximated sensitivity curve shown in Fig. 3 of [28]. Under this approximation, the wiggles in $f > f_*$ originated from the sinc function in \mathcal{T} have been smoothed out. As we can see, the frequency of the sensitivity curve can be divided into three regions: for $f < 10^{-2}$ Hz the curve is determined by the acceleration noise, such that the sensitivity is worsened as f^{-2} (according to Eq. 15); for 10^{-2} Hz $< f < f_* \approx 0.28$ Hz, i.e., the flat bottom, the curve is determined by the frequency independent position noise; for $f > f_*$ the curve is determined by $R(f)$.

4. Signal Simulation

Taking the reference source, J0806.3+1527, as an example, we simulate of the strain output from a single Michelson interferometer. The quadrupole formula provide the lowest-order post-Newtonian GW waveform for a binary system [53]

$$\begin{aligned} h_+(t) &= A (1 + \cos^2 \iota) \cos \Phi(t), \\ h_\times(t) &= 2A \cos \iota \sin \Phi(t). \end{aligned} \quad (18)$$

Here $A = 2(GM_c/c^2)^{5/3}(\pi f/c)^{2/3}/D_L$ is the GW overall amplitude, $M_c = 0.33 M_\odot$ (for component masses of $0.5 M_\odot$ and $0.25 M_\odot$) is the chirp mass, $D_L = 0.5$ kpc is the luminosity distance, $\iota = \pi/6$ is the inclination angle between the line of sight and the binary orbital axis, $\Phi(t)$ is the GW phase. For a space-based detector moving about the Sun, the GW phase can be given by [49]

$$\Phi(t) = 2\pi f t + 2\pi f(R/c) \cos \theta \cos(2\pi f_{\text{mt}} t - \phi) + \varphi_0, \quad (19)$$

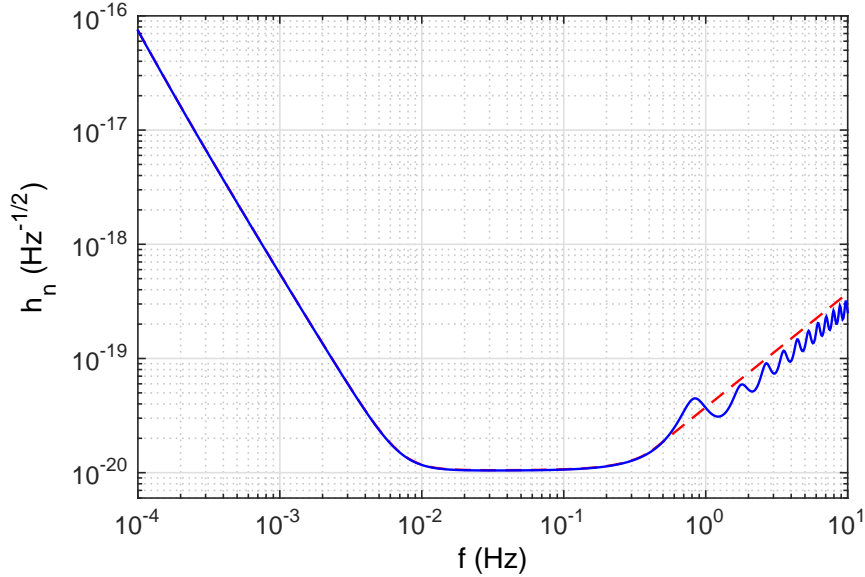


Figure 2. Sensitivity curve of TianQin. The blue solid line is the numerical evaluation of Eq. 16 over the interested frequency range. The red dash line is obtained from an analytic approximation. The two lines overlap for $f < f_* \approx 0.28$ Hz.

where φ_0 is the initial GW phase at the start of observation, $f = 6.22$ mHz is the GW frequency of the reference source, $R = 1$ AU, and (θ, ϕ) are the ecliptic coordinates of the source. $h_{+, \times}$ are calculated based on the physical parameters of the source in [44]. Here we ignore the evolution of f due to the GW emission from this system. The length of the simulation is one year.

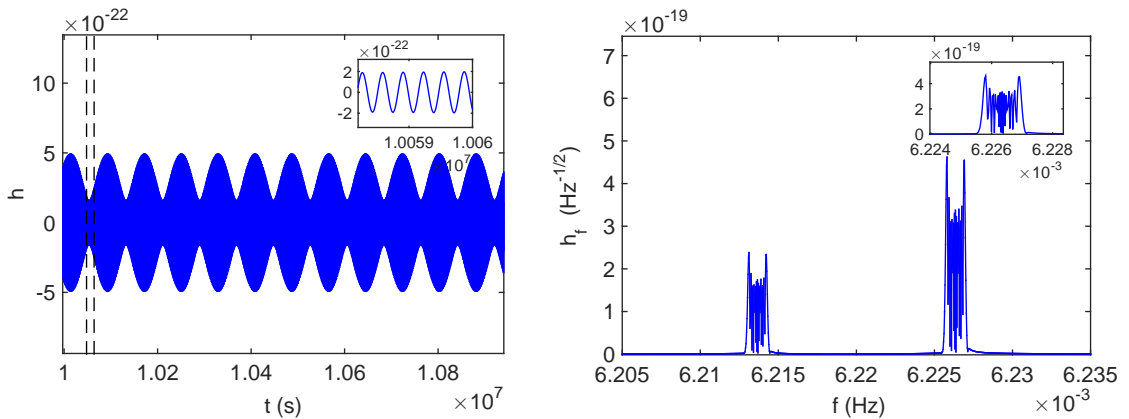


Figure 3. Left panel: Clip of the one-year noiseless time series of the strain output of a Michelson interferometer for GWs from the reference source. The inset zooms in of the data segment within the double dash lines. Right panel: ASD of the time series. The inset zooms in the right horn.

Shown in the left panel of Fig. 3 is the strain output data for about 11 days from one of the Michelson interferometers. The inset presents the sinusoidal signal of several cycles within the double dash lines. One can see that the overall amplitude (envelope)

of the signal is modulated by the antenna pattern being swept across the sky. The amplitude modulation frequency is $4f_{sc} \approx (0.9 \text{ day})^{-1}$, which follows the quadrupole characteristics of $F_i^{+,\times}$ in Eq. 13.

The phase of the signal is also modulated. This modulation is mainly caused by the differing time dependency of $F_i^{+,\times}$ which tunes the relative contribution of the two GW polarizations. In addition, phase modulation can also arise from the binary orbit axis precession, in which case the time-varying inclination angle ι alters the relative contribution. However, the orbital precession in general is negligible for white-dwarf binaries, therefore we do not consider this effect in the simulation.

Given in the right panel is the ASD h_f of the signal. It displays two horns, of which the centers are separated by about 1.3×10^{-5} Hz. This separation approximately equals to the modulation frequency of $4f_{sc}$ due to the antenna pattern functions. In other words, one can regard the signal amplitude modulation as a beat of two sinusoidal signals represented by the individual horns. The inset enlarges the horn on the right. The broadening of individual horn mainly results from the Doppler modulation of the detector's motion around the Sun. From Eq. 19, we find that, for this case, $\Delta f/f \leq 2\pi f_m(R/c) \approx 10^{-4}$, which makes $\Delta f \sim 6 \times 10^{-7}$ Hz.

5. Conclusion and Discussions

TianQin is a space-based laser interferometric gravitational wave detector aimed at detecting GWs in the low frequencies. It is formed by three drag-free spacecrafts orbiting around the Earth in an equilateral triangular constellation. The distance between a spacecraft and the center of the Earth is approximately 10^5 km. In this paper we provided the approximated analytic expressions for the coordinates of spacecraft's orbit in the heliocentric-ecliptic coordinate system. These expressions are sufficiently accurate and computationally efficient for the purpose of studying the scientific potential that can be enabled by TianQin as well as demonstrating and advancing the effectiveness of the data analysis techniques for various classes of GWs, such as compact white-dwarf binaries in the Galaxy, supermassive black hole binaries and extreme-mass-ratio inspirals (EMRIs), in a manner that is similar to the mock LISA data challenge [54].

Based on this analytic orbit we calculated the detector response of a single Michelson interferometer to plane GWs in arbitrary waveform. An example strain output for GWs from the reference white-dwarf binary is given which can be taken as the input of subsequent data analysis pipelines. Further investigations on simulating TDI data combinations and the associated sensitivities are currently in progress along with the development of the data analysis techniques that must content with it.

So far, the expression of the orbit does not include the perturbations from high order moments of the Earth, the Sun, the moon, planets, large asteroids, etc. The refinement of the coordinates and the numerical optimization of the orbit using numerical ephemerides [55] to reduce the arm length variation and range rate for TianQin will be subjected to our future work. One approach of refining coordinates

is to replace the initially selected values of the Keplerian orbit elements and the other variables used in Eq. 2 by the time-dependent values that are (perhaps piecewise) fitted from the numerical integration of the orbit. Initial investigation shows that, for example, θ_s and ϕ_s display both secular and periodic behaviors that represent the wobbling of the detector plane around the initial direction within several degrees during the mission lifetime. $\epsilon_n(t)$ in Eq. 1 will contain the residual coordinates after the fit. The alternative approach, which is through a brutal-force, is to use the numerical orbit directly. For this case, one needs to interpolate the numerical orbit with Legendre polynomials. This is owing to that the typical time step size adopted in the numerical integration of the orbit ($> 10^{-3}$ day) is much larger than the sampling time of the detector output (< 1 sec). Due to computational cost, this approach can be considered in a more matured stage of the system simulation when the highest accuracy is required. For the numerical integration of the orbit, the analytic coordinates can be used as a guidance for setting the initial values of spacecraft position and velocity. With the more accurate orbit, we can refine the simulations of the response and detector output presented in this paper.

The current work serves as our first step towards building a system-wide end-to-end model for TianQin. Work to integrate realistic noise components rooted from different subsystems, interplanetary and relativistic effects on the optical path, etc. will be subjected to our future study.

6. Acknowledgements

The authors thank the anonymous referees for helpful comments and suggestions. We would like to thank Prof. Soumya Mohanty for helpful comments and suggestions. Y.W. is supported by the National Natural Science Foundation of China under grants 91636111, 11690021 and 11503007. Y.M.H. acknowledges the support from the National Natural Science Foundation of China under grant 11703098.

7. References

- [1] B. P. Abbott, R. Abbott, T. D. Abbott, M. R. Abernathy, F. Acernese, K. Ackley, C. Adams, T. Adams, P. Addesso, R. X. Adhikari, and et al. Observation of Gravitational Waves from a Binary Black Hole Merger. *Physical Review Letters*, 116(6):061102, February 2016.
- [2] B. P. Abbott, R. Abbott, T. D. Abbott, M. R. Abernathy, F. Acernese, K. Ackley, C. Adams, T. Adams, P. Addesso, R. X. Adhikari, and et al. GW151226: Observation of Gravitational Waves from a 22-Solar-Mass Binary Black Hole Coalescence. *Physical Review Letters*, 116(24):241103, June 2016.
- [3] B. P. Abbott, R. Abbott, T. D. Abbott, F. Acernese, K. Ackley, C. Adams, T. Adams, P. Addesso, R. X. Adhikari, V. B. Adya, and et al. GW170814: A Three-Detector Observation of Gravitational Waves from a Binary Black Hole Coalescence. *Physical Review Letters*, 119(14):141101, October 2017.
- [4] B. P. Abbott, R. Abbott, T. D. Abbott, F. Acernese, K. Ackley, C. Adams, T. Adams, P. Addesso, R. X. Adhikari, V. B. Adya, and et al. GW170104: Observation of a 50-Solar-Mass Binary Black Hole Coalescence at Redshift 0.2. *Physical Review Letters*, 118(22):221101, June 2017.

- [5] B. P. Abbott, R. Abbott, T. D. Abbott, F. Acernese, K. Ackley, C. Adams, T. Adams, P. Addesso, R. X. Adhikari, V. B. Adya, and et al. GW170608: Observation of a 19 Solar-mass Binary Black Hole Coalescence. *The Astrophysical Journal Letters*, 851:L35, December 2017.
- [6] B. P. Abbott, R. Abbott, T. D. Abbott, F. Acernese, K. Ackley, C. Adams, T. Adams, P. Addesso, R. X. Adhikari, V. B. Adya, and et al. GW170817: Observation of Gravitational Waves from a Binary Neutron Star Inspiral. *Physical Review Letters*, 119(16):161101, October 2017.
- [7] F. Acernese, M. Agathos, K. Agatsuma, D. Aisa, N. Allemandou, A. Allocca, J. Amarni, P. Astone, G. Balestri, G. Ballardín, and et al. Advanced Virgo: a second-generation interferometric gravitational wave detector. *Classical and Quantum Gravity*, 32(2):024001, January 2015.
- [8] K. Somiya. Detector configuration of KAGRA-the Japanese cryogenic gravitational-wave detector. *Classical and Quantum Gravity*, 29(12):124007, June 2012.
- [9] C. S. Unnikrishnan. IndIGO and Ligo-India Scope and Plans for Gravitational Wave Research and Precision Metrology in India. *International Journal of Modern Physics D*, 22:1341010, January 2013.
- [10] M. Evans, L. Barsotti, P. Kwee, J. Harms, and H. Miao. Realistic filter cavities for advanced gravitational wave detectors. *Physical Review D*, 88(2):022002, July 2013.
- [11] J. Miller, L. Barsotti, S. Vitale, P. Fritschel, M. Evans, and D. Sigg. Prospects for doubling the range of Advanced LIGO. *Physical Review D*, 91(6):062005, March 2015.
- [12] S. Hild, M. Abernathy, F. Acernese, P. Amaro-Seoane, N. Andersson, K. Arun, F. Barone, B. Barr, M. Barsuglia, M. Beker, N. Beveridge, S. Birindelli, S. Bose, L. Bosi, S. Braccini, C. Bradaschia, T. Bulik, E. Calloni, G. Cella, E. Chassande Mottin, S. Chelkowski, A. Chincarini, J. Clark, E. Coccia, C. Colacino, J. Colas, A. Cumming, L. Cunningham, E. Cuoco, S. Danilishin, K. Danzmann, R. De Salvo, T. Dent, R. De Rosa, L. Di Fiore, A. Di Virgilio, M. Doets, V. Fafone, P. Falferi, R. Flaminio, J. Franc, F. Frasconi, A. Freise, D. Friedrich, P. Fulda, J. Gair, G. Gemme, E. Genin, A. Gennai, A. Giazotto, K. Glampedakis, C. Gräf, M. Granata, H. Grote, G. Guidi, A. Gurkovsky, G. Hammond, M. Hannam, J. Harms, D. Heinert, M. Hendry, I. Heng, E. Hennes, J. Hough, S. Husa, S. Huttner, G. Jones, F. Khalili, K. Kokeyama, K. Kokkotas, B. Krishnan, T. G. F. Li, M. Lorenzini, H. Lück, E. Majorana, I. Mandel, V. Mandic, M. Mantovani, I. Martin, C. Michel, Y. Minenkov, N. Morgado, S. Mosca, B. Mours, H. Müller-Ebhardt, P. Murray, R. Nawrodt, J. Nelson, R. Oshaughnessy, C. D. Ott, C. Palomba, A. Paoli, G. Parguez, A. Pasqualetti, R. Passaquieti, D. Passuello, L. Pinard, W. Plastino, R. Poggiani, P. Popolizio, M. Prato, M. Punturo, P. Puppò, D. Rabeling, P. Rapagnani, J. Read, T. Regimbau, H. Rehbein, S. Reid, F. Ricci, F. Richard, A. Rocchi, S. Rowan, A. Rüdiger, L. Santamaría, B. Sassolas, B. Sathyaprakash, R. Schnabel, C. Schwarz, P. Seidel, A. Sintes, K. Somiya, F. Speirits, K. Strain, S. Strigin, P. Sutton, S. Tarabrin, A. Thüring, J. van den Brand, M. van Veggel, C. van den Broeck, A. Vecchio, J. Veitch, F. Vetrano, A. Vicere, S. Vyatchanin, B. Willke, G. Woan, and K. Yamamoto. Sensitivity studies for third-generation gravitational wave observatories. *Classical and Quantum Gravity*, 28(9):094013, May 2011.
- [13] B. P. Abbott, R. Abbott, T. D. Abbott, M. R. Abernathy, K. Ackley, C. Adams, P. Addesso, R. X. Adhikari, V. B. Adya, C. Affeldt, and et al. Exploring the sensitivity of next generation gravitational wave detectors. *Classical and Quantum Gravity*, 34(4):044001, February 2017.
- [14] R. M. Shannon, V. Ravi, L. T. Lentati, P. D. Lasky, G. Hobbs, M. Kerr, R. N. Manchester, W. A. Coles, Y. Levin, M. Bailes, N. D. R. Bhat, S. Burke-Spolaor, S. Dai, M. J. Keith, S. Osłowski, D. J. Reardon, W. van Straten, L. Toomey, J.-B. Wang, L. Wen, J. S. B. Wyithe, and X.-J. Zhu. Gravitational waves from binary supermassive black holes missing in pulsar observations. *Science*, 349:1522–1525, September 2015.
- [15] L. Lentati, S. R. Taylor, C. M. F. Mingarelli, A. Sesana, S. A. Sanidas, A. Vecchio, R. N. Caballero, K. J. Lee, R. van Haasteren, S. Babak, C. G. Bassa, P. Brem, M. Burgay, D. J. Champion, I. Cognard, G. Desvignes, J. R. Gair, L. Guillemot, J. W. T. Hessels, G. H. Janssen, R. Karuppusamy, M. Kramer, A. Lassis, P. Lazarus, K. Liu, S. Osłowski, D. Perrodin, A. Petiteau, A. Possenti, M. B. Purver, P. A. Rosado, R. Smits, B. Stappers, G. Theureau,

- C. Tiburzi, and J. P. W. Verbiest. European Pulsar Timing Array limits on an isotropic stochastic gravitational-wave background. *Monthly Notices of the Royal Astronomical Society*, 453:2576–2598, November 2015.
- [16] Z. Arzoumanian, A. Brazier, S. Burke-Spolaor, S. J. Chamberlin, S. Chatterjee, B. Christy, J. M. Cordes, N. J. Cornish, K. Crowter, P. B. Demorest, X. Deng, T. Dolch, J. A. Ellis, R. D. Ferdman, E. Fonseca, N. Garver-Daniels, M. E. Gonzalez, F. Jenet, G. Jones, M. L. Jones, V. M. Kaspi, M. Koop, M. T. Lam, T. J. W. Lazio, L. Levin, A. N. Lommen, D. R. Lorimer, J. Luo, R. S. Lynch, D. R. Madison, M. A. McLaughlin, S. T. McWilliams, C. M. F. Mingarelli, D. J. Nice, N. Palliyaguru, T. T. Pennucci, S. M. Ransom, L. Sampson, S. A. Sanidas, A. Sesana, X. Siemens, J. Simon, I. H. Stairs, D. R. Stinebring, K. Stovall, J. Swiggum, S. R. Taylor, M. Vallisneri, R. van Haasteren, Y. Wang, W. W. Zhu, and The NANOGrav Collaboration. The NANOGrav Nine-year Data Set: Limits on the Isotropic Stochastic Gravitational Wave Background. *The Astrophysical Journal*, 821:13, April 2016.
- [17] Z. Arzoumanian, A. Brazier, S. Burke-Spolaor, S. J. Chamberlin, S. Chatterjee, J. M. Cordes, P. B. Demorest, X. Deng, T. Dolch, J. A. Ellis, R. D. Ferdman, N. Garver-Daniels, F. Jenet, G. Jones, V. M. Kaspi, M. Koop, M. T. Lam, T. J. W. Lazio, A. N. Lommen, D. R. Lorimer, J. Luo, R. S. Lynch, D. R. Madison, M. A. McLaughlin, S. T. McWilliams, D. J. Nice, N. Palliyaguru, T. T. Pennucci, S. M. Ransom, A. Sesana, X. Siemens, I. H. Stairs, D. R. Stinebring, K. Stovall, J. Swiggum, M. Vallisneri, R. van Haasteren, Y. Wang, W. W. Zhu, and NANOGrav Collaboration. Gravitational Waves from Individual Supermassive Black Hole Binaries in Circular Orbits: Limits from the North American Nanohertz Observatory for Gravitational Waves. *The Astrophysical Journal*, 794:141, October 2014.
- [18] X.-J. Zhu, G. Hobbs, L. Wen, W. A. Coles, J.-B. Wang, R. M. Shannon, R. N. Manchester, M. Bailes, N. D. R. Bhat, S. Burke-Spolaor, S. Dai, M. J. Keith, M. Kerr, Y. Levin, D. R. Madison, S. Osłowski, V. Ravi, L. Toomey, and W. van Straten. An all-sky search for continuous gravitational waves in the Parkes Pulsar Timing Array data set. *Monthly Notices of the Royal Astronomical Society*, 444:3709–3720, November 2014.
- [19] S. Babak, A. Petiteau, A. Sesana, P. Brem, P. A. Rosado, S. R. Taylor, A. Lassus, J. W. T. Hessels, C. G. Bassa, M. Burgay, R. N. Caballero, D. J. Champion, I. Cognard, G. Desvignes, J. R. Gair, L. Guillemot, G. H. Janssen, R. Karuppusamy, M. Kramer, P. Lazarus, K. J. Lee, L. Lentati, K. Liu, C. M. F. Mingarelli, S. Osłowski, D. Perrodin, A. Possenti, M. B. Purver, S. Sanidas, R. Smits, B. Stappers, G. Theureau, C. Tiburzi, R. van Haasteren, A. Vecchio, and J. P. W. Verbiest. European Pulsar Timing Array limits on continuous gravitational waves from individual supermassive black hole binaries. *Monthly Notices of the Royal Astronomical Society*, 455:1665–1679, January 2016.
- [20] G. Hobbs, S. Dai, R. N. Manchester, R. M. Shannon, M. Kerr, K. J. Lee, and R. Xu. The Role of FAST in Pulsar Timing Arrays. *ArXiv e-prints*, July 2014.
- [21] Y. Wang and S. D. Mohanty. Pulsar Timing Array Based Search for Supermassive Black Hole Binaries in the Square Kilometer Array Era. *Physical Review Letters*, 118(15):151104, April 2017.
- [22] Y. Wang and S. D. Mohanty. Prospects for gravitational wave astronomy with next generation large-scale pulsar timing arrays. *ArXiv e-prints*, November 2017.
- [23] J. E. Faller, P. L. Bender, J. L. Hall, D. Hils, and M. A. Vincent. Space antenna for gravitational wave astronomy. In N. Longdon and O. Melita, editors, *Kilometric Optical Arrays in Space*, volume 226 of *ESA Special Publication*, April 1985.
- [24] B. S. Sathyaprakash and Bernard F. Schutz. Physics, astrophysics and cosmology with gravitational waves. *Living Reviews in Relativity*, 12(1):2, Mar 2009.
- [25] P. Amaro-Seoane, H. Audley, S. Babak, J. Baker, E. Barausse, P. Bender, E. Berti, P. Binetruy, M. Born, D. Bortoluzzi, J. Camp, C. Caprini, V. Cardoso, M. Colpi, J. Conklin, N. Cornish, C. Cutler, K. Danzmann, R. Dolesi, L. Ferraioli, V. Ferroni, E. Fitzsimons, J. Gair, L. Gesa Bote, D. Giardini, F. Gibert, C. Grmani, H. Halloin, G. Heinzl, T. Hertog, M. Hewitson,

- K. Holley-Bockelmann, D. Hollington, M. Hueller, H. Inchauspe, P. Jetzer, N. Karnesis, C. Killow, A. Klein, B. Klipstein, N. Korsakova, S. L Larson, J. Livas, I. Lloro, N. Man, D. Mance, J. Martino, I. Mateos, K. McKenzie, S. T McWilliams, C. Miller, G. Mueller, G. Nardini, G. Nelemans, M. Nofrarias, A. Petiteau, P. Pivato, E. Plagnol, E. Porter, J. Reiche, D. Robertson, N. Robertson, E. Rossi, G. Russano, B. Schutz, A. Sesana, D. Shoemaker, J. Slutsky, C. F. Sopuerta, T. Sumner, N. Tamanini, I. Thorpe, M. Troebs, M. Vallisneri, A. Vecchio, D. Vetrugno, S. Vitale, M. Volonteri, G. Wanner, H. Ward, P. Wass, W. Weber, J. Ziemer, and P. Zweifel. Laser Interferometer Space Antenna. *ArXiv e-prints*, February 2017.
- [26] P. A. Seoane, S. Aoudia, H. Audley, G. Auger, and et al. The Gravitational Universe. *ArXiv e-prints*, May 2013.
- [27] M. Armano, H. Audley, G. Auger, J. T. Baird, M. Bassan, P. Binetruy, M. Born, D. Bortoluzzi, N. Brandt, M. Caleno, L. Carbone, A. Cavalleri, A. Cesarini, G. Ciani, G. Congedo, A. M. Cruise, K. Danzmann, and et al. Sub-femto- g free fall for space-based gravitational wave observatories: Lisa pathfinder results. *Phys. Rev. Lett.*, 116:231101, Jun 2016.
- [28] J. Luo, L.-S. Chen, H.-Z. Duan, Y.-G. Gong, S. Hu, J. Ji, Q. Liu, J. Mei, V. Milyukov, M. Sazhin, C.-G. Shao, V. T. Toth, H.-B. Tu, Y. Wang, Y. Wang, H.-C. Yeh, M.-S. Zhan, Y. Zhang, V. Zharov, and Z.-B. Zhou. TianQin: a space-borne gravitational wave detector. *Classical and Quantum Gravity*, 33(3):035010, February 2016.
- [29] S. Sato, S. Kawamura, M. Ando, T. Nakamura, K. Tsubono, A. Araya, I. Funaki, K. Ioka, N. Kanda, S. Moriwaki, M. Musha, K. Nakazawa, K. Numata, S.-i. Sakai, N. Seto, T. Takashima, T. Tanaka, K. Agatsuma, K.-s. Aoyanagi, K. Arai, H. Asada, Y. Aso, T. Chiba, T. Ebisuzaki, Y. Ejiri, M. Enoki, Y. Eriguchi, M.-K. Fujimoto, R. Fujita, M. Fukushima, T. Futamase, K. Ganzu, T. Harada, T. Hashimoto, K. Hayama, W. Hikida, Y. Himemoto, H. Hirabayashi, T. Hiramatsu, F.-L. Hong, H. Horisawa, M. Hosokawa, K. Ichiki, T. Ikegami, K. T. Inoue, K. Ishidoshiro, H. Ishihara, T. Ishikawa, H. Ishizaki, H. Ito, Y. Itoh, N. Kawashima, F. Kawazoe, N. Kishimoto, K. Kiuchi, S. Kobayashi, K. Kohri, H. Koizumi, Y. Kojima, K. Kokeyama, W. Kokuyama, K. Kotake, Y. Kozai, H. Kudoh, H. Kunimori, H. Kunitaka, K. Kuroda, K.-i. Maeda, H. Matsuhara, Y. Mino, O. Miyakawa, S. Miyoki, M. Y. Morimoto, T. Morioka, T. Morisawa, S. Mukohyama, S. Nagano, I. Naito, K. Nakamura, H. Nakano, K. Nakao, S. Nakasuka, Y. Nakayama, E. Nishida, K. Nishiyama, A. Nishizawa, Y. Niwa, T. Noumi, Y. Obuchi, M. Ohashi, N. Ohishi, M. Ohkawa, N. Okada, K. Onozato, K. Oohara, N. Sago, M. Saijo, M. Sakagami, S. Sakata, M. Sasaki, T. Sato, M. Shibata, H. Shinkai, K. Somiya, H. Sotani, N. Sugiyama, Y. Suwa, R. Suzuki, H. Tagoshi, F. Takahashi, K. Takahashi, K. Takahashi, R. Takahashi, R. Takahashi, T. Takahashi, H. Takahashi, T. Akiteru, T. Takano, K. Taniguchi, A. Taruya, H. Tashiro, Y. Torii, M. Toyoshima, S. Tsujikawa, Y. Tsunesada, A. Ueda, K.-i. Ueda, M. Utashima, Y. Wakabayashi, H. Yamakawa, K. Yamamoto, T. Yamazaki, J. Yokoyama, C.-M. Yoo, S. Yoshida, and T. Yoshino. DECIGO: The Japanese space gravitational wave antenna. *Journal of Physics Conference Series*, 154(1):012040, March 2009.
- [30] M Tinto, J. C. N De Araujo, O. D Aguiar, and M. E. S Alves. Searching for gravitational waves with a geostationary gravitational wave interferometer. *Astroparticle Physics*, 48(5):50–60, 2011.
- [31] M. Tinto, D. Debra, S. Buchman, and S. Tilley. glisa: geosynchronous laser interferometer space antenna concepts with off-the-shelf satellites. *Review of Scientific Instruments*, 86(1):330, 2015.
- [32] W.-T. Ni. ASTROD-An Overview. *International Journal of Modern Physics D*, 11:947–962, 2002.
- [33] Wei Tou Ni, Junwei Cao, Hansjoerg Dittus, Peng Dong, Jian Guo, Claus Laemmerzahl, Xiaohong Mei, Diana Shaul, T. J Sumner, and Gang Wang. Astrod optimized for gravitational wave detection: Astrod-gw. *Silva Lusitana*, 13(9):246–253, 2009.
- [34] X. Gong, Y.-K. Lau, S. Xu, P. Amaro-Seoane, S. Bai, X. Bian, Z. Cao, G. Chen, X. Chen, Y. Ding, P. Dong, W. Gao, G. Heinzel, M. Li, S. Li, F. Liu, Z. Luo, M. Shao, R. Spurzem, B. Sun, W. Tang, Y. Wang, P. Xu, P. Yu, Y. Yuan, X. Zhang, and Z. Zhou. Descope of the ALIA mission. In *Journal of Physics Conference Series*, volume 610 of *Journal of Physics Conference Series*, page 012011, May 2015.

- [35] C. Cutler and J. Harms. Bbo and the neutron-star-binary subtraction problem. *Physics*, 73(4):1405–1408, 2006.
- [36] Jeff Crowder and Neil J. Cornish. Beyond lisa: Exploring future gravitational wave missions. *Physical Review D Particles Fields*, 72(8):344–344, 2005.
- [37] B Hiscock and R. W Hellings. Omega: a space gravitational wave midex mission. In *Bulletin of the American Astronomical Society*, page 1312, 1997.
- [38] J. W. Conklin, S. Buchman, V. Aguero, A. Alfauwaz, A. Aljadaan, M. Almajed, H. Altwaijry, T. Alsaud, K. Balakrishnan, and R. L. Byer. Lagrange: Laser gravitational-wave antenna at geo-lunar lagrange points. *Eprint Arxiv*, 2011.
- [39] W.-T. Ni. Gravitational wave detection in space. *International Journal of Modern Physics D*, 25:1630001–129, 2016.
- [40] S. M. Merkowitz. The LISA integrated model. *Classical and Quantum Gravity*, 20:S255–S260, May 2003.
- [41] S. V. Dhurandhar, K. R. Nayak, S. Koshti, and J.-Y. Vinet. Fundamentals of the LISA stable flight formation. *Classical and Quantum Gravity*, 22:481–487, February 2005.
- [42] B. Chauvineau, T. Regimbau, J.-Y. Vinet, and S. Pireaux. Relativistic analysis of the LISA long range optical links. *Physical Review D*, 72(12):122003, December 2005.
- [43] M. Tinto and S. V. Dhurandhar. Time-Delay Interferometry. *Living Reviews in Relativity*, 8:4, July 2005.
- [44] Gijs H. A. Roelofs, Arne Rau, Tom R. Marsh, Danny Steeghs, Paul J. Groot, and Gijs Nelemans. Spectroscopic evidence for a 5.4 minute orbital period in hm cancri. *The Astrophysical Journal Letters*, 711(2):L138, 2010.
- [45] A. Petiteau, G. Auger, H. Halloin, O. Jeannin, E. Plagnol, S. Pireaux, T. Regimbau, and J.-Y. Vinet. LISACode: A scientific simulator of LISA. *Physical Review D*, 77(2):023002, January 2008.
- [46] Yi-Ming Hu, Jianwei Mei, and Jun Luo. Science prospects for space-borne gravitational-wave missions. *National Science Review*, 4(5):683–684, 2017.
- [47] K. S. Thorne. *Gravitational radiation.*, pages 330–458. 1987.
- [48] N. J. Cornish and L. J. Rubbo. LISA response function. *Physical Review D*, 67(2):022001, January 2003.
- [49] L. J. Rubbo, N. J. Cornish, and O. Poujade. Forward modeling of space-borne gravitational wave detectors. *Physical Review D*, 69(8):082003, April 2004.
- [50] B. S. Sathyaprakash and B. F. Schutz. Physics, Astrophysics and Cosmology with Gravitational Waves. *Living Reviews in Relativity*, 12:2, December 2009.
- [51] F. Hechler and W. M. Folkner. Mission analysis for the Laser Interferometer Space Antenna (LISA) mission. *Advances in Space Research*, 32:1277–1282, October 2003.
- [52] Neil J Cornish and Shane L Larson. Space missions to detect the cosmic gravitational-wave background. *Classical and Quantum Gravity*, 18(17):3473, 2001.
- [53] M. Maggiore. *Gravitational Waves: Volume 1: Theory and Experiments*. Oxford University Press, 2007.
- [54] K. A. Arnaud, S. Babak, J. G. Baker, M. J. Benacquista, N. J. Cornish, C. Cutler, L. S. Finn, S. L. Larson, T. Littenberg, E. K. Porter, M. Vallisneri, A. Vecchio, J.-Y. Vinet, and T. M. L. Data Challenge Task Force. An overview of the second round of the Mock LISA Data Challenges. *Classical and Quantum Gravity*, 24:S551–S564, October 2007.
- [55] G. Wang and W.-T. Ni. Numerical simulation of time delay interferometry for eLISA/NGO. *Classical and Quantum Gravity*, 30(6):065011, March 2013.

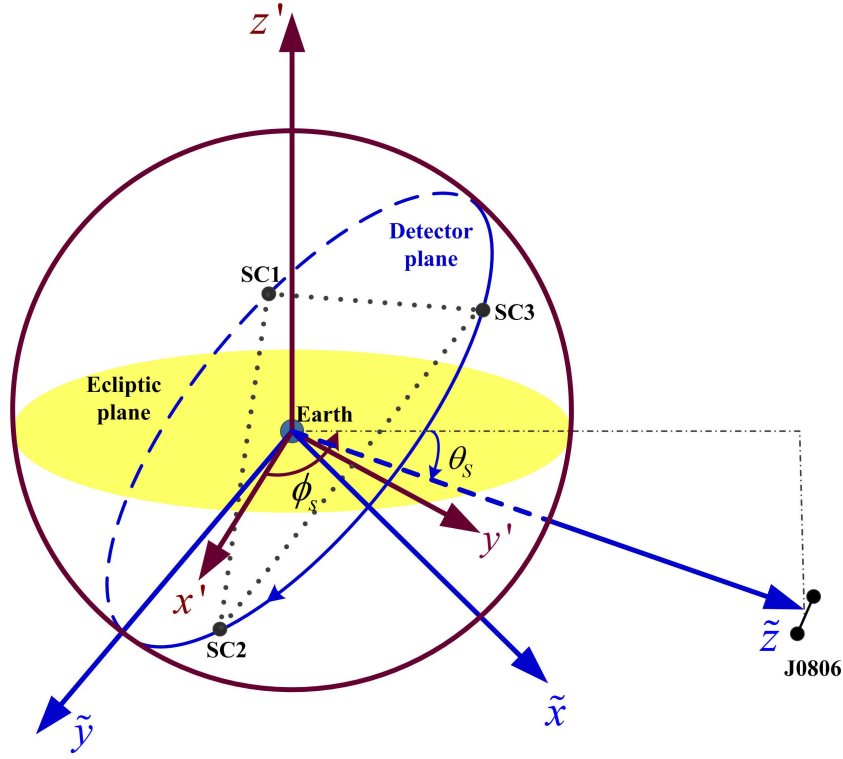


Figure A1. Schematic of the detector coordinate system $\{\tilde{x}, \tilde{y}, \tilde{z}\}$ and the geocentric-ecliptic coordinate system $\{x', y', z'\}$. \tilde{x} and \tilde{y} axes point toward the descending node and the lowest point of the detector plane relative to the ecliptic plane, respectively. \tilde{z} axis points toward the orbital angular momentum of spacecraft which is along the direction of the reference source (ϕ_s, θ_s) . $\{x', y', z'\}$ are respectively parallel to the $\{x, y, z\}$ in the heliocentric-ecliptic coordinate system shown in Fig. 1. Dot lines represent the optical links between each pair of spacecraft.

Appendix A. The coordinates of the TianQin spacecraft

We start with the Cartesian coordinates for the guiding center of the spacecraft constellation, i.e., the geocenter, in the heliocentric-ecliptic coordinate system,

$$\begin{aligned} X &= r \cos \gamma, \\ Y &= r \sin \gamma, \\ Z &= 0, \end{aligned} \tag{A.1}$$

where γ is the true anomaly, r is the Keplerian radius

$$r = \frac{R(1 - e^2)}{1 + e \cos \gamma}. \tag{A.2}$$

Here $R = 1$ AU, $e = 0.0167$ is the eccentricity of the Earth orbit. The relation between γ and the eccentric anomaly ψ is

$$\tan \frac{\gamma}{2} = \sqrt{\frac{1+e}{1-e}} \tan \frac{\psi}{2}, \tag{A.3}$$

and the relation between ψ and the mean anomaly M is

$$\psi - e \sin \psi = M = 2\pi f_m(t - \tau). \quad (\text{A.4})$$

In the second equality, M is expressed in terms of the geocenter orbit modulation frequency $f_m = 1/(\text{one sidereal year}) = 3.14 \times 10^{-8}$ Hz and the passing time of the perihelion τ . In practice, it is more convenient to express ψ by the mean orbital ecliptic longitude $\alpha(t)$, which is

$$\psi - e \sin \psi = \alpha(t) - \beta, \quad (\text{A.5})$$

where $\alpha(t) = 2\pi f_m t + \kappa_0$, κ_0 is the mean ecliptic longitude measured from the vernal equinox at $t = 0$, and β is the angle measured from the vernal equinox to the perihelion (see Fig. 1). Eq. A.5 is a transcendental equation which is usually solved by iterative method. Given $e \ll 1$, ψ can be iteratively expanded up to any order of e , the expression to the second order is given by

$$\psi = \alpha - \beta + e \sin(\alpha - \beta) + e^2 \cos(\alpha - \beta) \sin(\alpha - \beta) + \text{O}(e^3). \quad (\text{A.6})$$

Next, inserting Eq. A.6 into Eq. A.3, we find the expression of γ in terms of $\alpha - \beta$ up to the second order of e

$$\gamma = \alpha - \beta + 2e \sin(\alpha - \beta) + \frac{5}{2}e^2 \cos(\alpha - \beta) \sin(\alpha - \beta) + \text{O}(e^3). \quad (\text{A.7})$$

The coordinates of the geocenter can be obtained by substituting Eq. A.2 and Eq. A.7 into Eq. A.1, which are

$$\begin{aligned} X(t) &= R \cos(\alpha - \beta) + \frac{1}{2}eR(\cos 2(\alpha - \beta) - 3) - \frac{3}{2}e^2R \cos(\alpha - \beta) \sin^2(\alpha - \beta) + \text{O}(e^3), \\ Y(t) &= R \sin(\alpha - \beta) + \frac{1}{2}eR \sin 2(\alpha - \beta) + \frac{1}{4}e^2R \sin(\alpha - \beta)(3 \cos 2(\alpha - \beta) - 1) + \text{O}(e^3), \\ Z(t) &= 0. \end{aligned} \quad (\text{A.8})$$

In the detector plane spanned by \tilde{x} and \tilde{y} axes shown in Fig. A1, each spacecraft revolves around the geocenter in a Keplerian orbit. We follow the same procedure as above to obtain its analytic coordinates in the detector coordinate system $\{\tilde{x}, \tilde{y}, \tilde{z}\}$. For the n -th ($n = 1, 2, 3$) spacecraft

$$\begin{aligned} \tilde{x}_n(t) &= R_1 \cos(\alpha_n - \beta') + \frac{1}{2}e_1 R_1 (\cos 2(\alpha_n - \beta') - 3) - \frac{3}{2}e_1^2 R_1 \cos(\alpha_n - \beta') \sin^2(\alpha_n - \beta') + \text{O}(e_1^3), \\ \tilde{y}_n(t) &= R_1 \sin(\alpha_n - \beta') + \frac{1}{2}e_1 R_1 \sin 2(\alpha_n - \beta') + \frac{1}{4}e_1^2 R_1 \sin(\alpha_n - \beta') (3 \cos 2(\alpha_n - \beta') - 1) + \text{O}(e_1^3), \\ \tilde{z}_n(t) &= 0. \end{aligned} \quad (\text{A.9})$$

Here e_1 is the eccentricity and $R_1 = 1.0 \times 10^5$ km is the semi-major axis of the spacecraft orbit. The spacecraft orbit phase α_n is

$$\alpha_n(t) = 2\pi f_{sc} t + \kappa_n, \quad (\text{A.10})$$

where $\kappa_n = \frac{2\pi}{3}(n-1) + \lambda$, λ is the initial orbit phase of the first ($n=1$) spacecraft measured from \tilde{x} axis. $f_{sc} \approx 1/(3.65 \text{ day})$ is the modulation frequency due to the rotation of the detector around the guiding center. β' is the angle measured from the \tilde{x} axis to the perigee of the spacecraft orbit.

According to the relation illustrated in Fig. A1, we translate the coordinates $\{\tilde{x}_n, \tilde{y}_n, \tilde{z}_n\}$ in the detector coordinate system into the geocentric-ecliptic coordinate system. This can be done by applying two rotation matrices as below

$$\begin{pmatrix} x'_n \\ y'_n \\ z'_n \end{pmatrix} = \begin{pmatrix} \sin \phi_s & \cos \phi_s & 0 \\ -\cos \phi_s & \sin \phi_s & 0 \\ 0 & 0 & 1 \end{pmatrix} \begin{pmatrix} 1 & 0 & 0 \\ 0 & \sin \theta_s & \cos \theta_s \\ 0 & -\cos \theta_s & \sin \theta_s \end{pmatrix} \begin{pmatrix} \tilde{x}_n \\ \tilde{y}_n \\ \tilde{z}_n \end{pmatrix}. \quad (\text{A.11})$$

Here $\phi_s = 120.5^\circ$ and $\theta_s = -4.7^\circ$ are the ecliptic longitude and latitude of the reference source J0806.3+1527, respectively. Explicitly, the coordinates of the n -th spacecraft in the geocentric-ecliptic coordinate system can be written as

$$\begin{aligned} x'_n(t) &= R_1 (\cos \phi_s \sin \theta_s \sin(\alpha_n - \beta') + \cos(\alpha_n - \beta') \sin \phi_s) + R_1 e_1 \left[\frac{1}{2} (\cos 2(\alpha_n - \beta') - 3) \sin \phi_s \right. \\ &\quad \left. + \cos(\alpha_n - \beta') \cos \phi_s \sin \theta_s \sin(\alpha_n - \beta') \right] + \frac{e_1^2}{4} R_1 \sin(\alpha_n - \beta') \left[(3 \cos 2(\alpha_n - \beta') - 1) \right. \\ &\quad \left. \times \cos \phi_s \sin \theta_s - 6 \cos(\alpha_n - \beta') \sin(\alpha_n - \beta') \sin \phi_s \right] + O(e_1^3), \\ y'_n(t) &= R_1 (\sin \phi_s \sin \theta_s \sin(\alpha_n - \beta') - \cos(\alpha_n - \beta') \cos \phi_s) + R_1 e_1 \left[-\frac{1}{2} (\cos 2(\alpha_n - \beta') - 3) \cos \phi_s \right. \\ &\quad \left. + \cos(\alpha_n - \beta') \sin \phi_s \sin \theta_s \sin(\alpha_n - \beta') \right] + \frac{e_1^2}{4} R_1 \sin(\alpha_n - \beta') \left[(3 \cos 2(\alpha_n - \beta') - 1) \right. \\ &\quad \left. \times \sin \phi_s \sin \theta_s + 6 \cos(\alpha_n - \beta') \sin(\alpha_n - \beta') \cos \phi_s \right] + O(e_1^3), \\ z'_n(t) &= -R_1 \sin(\alpha_n - \beta') \cos \theta_s - R_1 e_1 \cos(\alpha_n - \beta') \sin(\alpha_n - \beta') \cos \theta_s \\ &\quad - \frac{1}{4} e_1^2 R_1 (3 \cos 2(\alpha_n - \beta') - 1) \sin(\alpha_n - \beta') \cos \theta_s + O(e_1^3). \end{aligned} \quad (\text{A.12})$$

Finally, the coordinates of the spacecraft in Eq. 2 can be easily found by adding Eq. A.8 and Eq. A.12 together. Note that we have only kept up to the second order of e and e_1 . Higher order terms can be straightforwardly obtained.